Article

pubs.acs.org/Biomac

Fabrication of Biomaterials via Controlled Protein Bubble Generation and Manipulation

Zeynep Ekemen,[†] Hong Chang,[‡] Zeeshan Ahmad,*[,§] Cem Bayram,[∥] Zimei Rong,[‡] Emir Baki Denkbas,[∥] Eleanor Stride,[†] Pankaj Vadgama,[‡] and Mohan Edirisinghe[†]

[†]Department of Mechanical Engineering, University College London, Torrington Place, London WC1E 7JE, United Kingdom

[‡]IRC in Biomedical Materials, Queen Mary University of London, Mile End Road, London E1 4NS, United Kingdom

[§]School of Pharmacy and Biomedical Sciences, University of Portsmouth, St Michael's Building, White Swan Road, Portsmouth, PO1 2DT, United Kingdom

[∥]Nanotechnology and Nanomedicine Division, The Institute For Graduate Studies in Science and Engineering, Hacettepe University, 06800, Ankara, Turkey

ABSTRACT: In this work, we utilize a recently developed microbubbling process to generate controlled protein (bovine serum albumin, BSA) coated bubbles and then manipulate these to fabricate a variety of structures suitable for several generic biomedical applications, tissue engineering, and biosensor coatings. Using BSA solutions with varying concentrations (20, 25, and 30 wt %) and cross-linking (terephthaloyl chloride) mechanisms, structures were fabricated including porous thin films with variable pore sizes and thickness (partially cross-linked coupled to bubble breakdown), scaffolds with variable pore morphologies (fully cross-linked), and coated bubbles (no cross-linking), which can be used as stand-alone delivery devices and contrast agents. The movement of typical biosensor chemicals (catechol and hydrogen peroxide) across appropriate film structures was studied. The potential of formed scaffold structures for tissue engineering applications was demonstrated using mouse cell lines (L929). In addition to low cost, providing uniform structure generation and high output, the size of the bubbles can easily be controlled by adjusting simplistic processing parameters. The combination of robust processing and chemical modification to uniform macromolecule bubbles can be utilized as a competing, yet novel, tool with current technologies and processes in advancing the biomaterials and biomedical engineering remits.

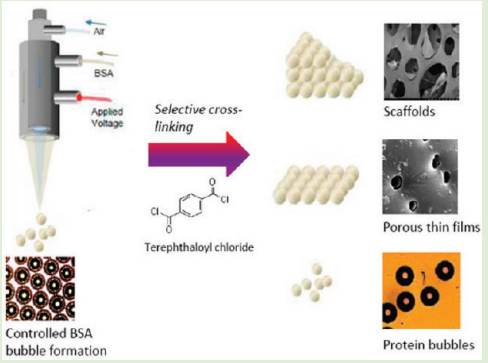

INTRODUCTION

Fabrication of highly ordered and uniform biomacromolecule structures is desirable in several branches of both established and emerging biomedical fields, for example, tissue engineering (scaffolds), thin film (coatings), membranes, drug delivery, and medical imaging.[1−3] To reproduce systematically architectures, on both the micro- and nanometer scales, we often utilize various forms of templates,[4−6] and the overall fabrication process generally consists of numerous steps. Alternatively, lithography and etching can also be deployed, which can result in forming of materials with excellent attention to detail.

More specifically, several material processes can be deployed to generate porous 3D structures including particulate leaching,[7] emulsification,[8] freeze-casting,[9] direct-writing,[10] phase separation,[11] and several other routes utilizing fibers.[12] However, these have limitations such as loss of reagent (between steps) and an increase in overall forming time, which can significantly reduce the economic benefit when compared with a single step or in-situ forming process. However, with regard to fabrication of porous 3D structures, templating methods, largely because of the innate structure of the substrate or particle system and the corresponding formed structure, provide little compromise between template and resulting architectures, and so conventional methods of this nature result in solitary structures. However, more sophisticated templating methods, or templates, where there is fine control of desirable variations in the outputs, driven by an intended application, are a challenge (e.g., size, shape, morphology, porosity, etc.). One way to achieve this is to combine templating methods with complementary processes, for example, chemical modifications, which can result in the formation of structures driven by external variables or triggers.

In addition to salt leaching and phase separation methods, the use of gaseous systems (e.g., bubbles) to serve as porosifying agents has been identified[13] and has several benefits such as limiting the loss of reagent due to leaching and solvent-free pore generation. However, with such methods, there still remains a lack of control over several structural aspects (e.g., porosity and ordering) as gaseous vesicles produced using conventional methods, such as sonication, are highly

Received: August 28, 2011
Revised: October 15, 2011
Published: November 1, 2011

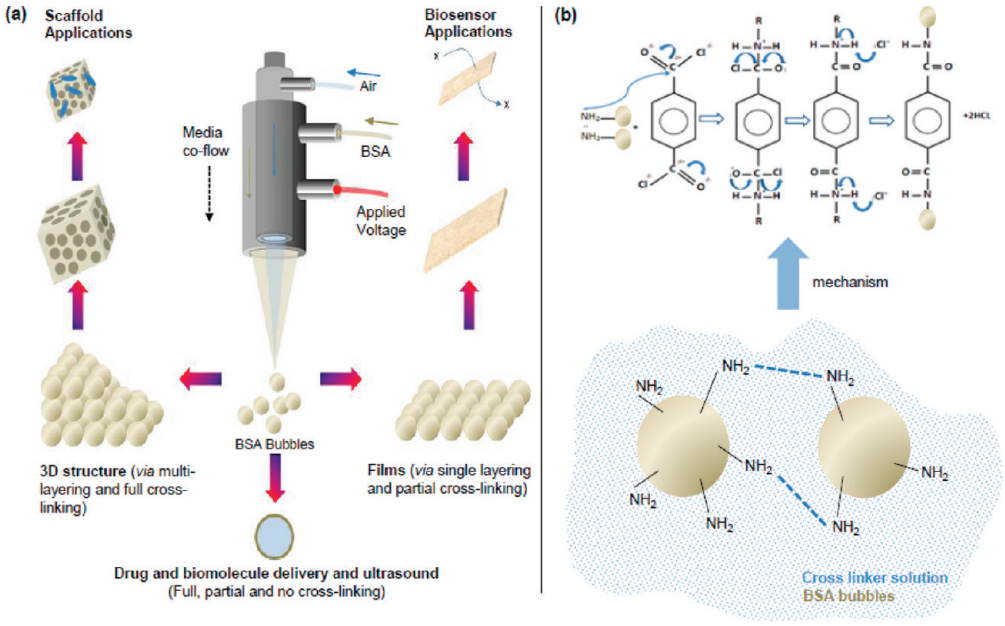

Figure 1. (a) Schematic showing experimental sequences and (b) coupling mechanism for BSA protein bubbles in the forming of protein-based biomaterial structures.

polydispersed.[14,15] In contrast, methods such as microfluidics, which boast excellent control over size distribution, fall short in output/production rates. To enable the utilization of such structures on commercially impacting scales, output and forming control cues are crucial.

As is the case with most material forming technologies, several processes exist to generate desired bubble structures. For bubble systems, in addition to those methods aforementioned, a recently developed electric-field-assisted method demonstrates potential to attain conformity between size and output rates.[16] Namely, coaxial electrohydrodynamic forming, also referred to as coaxial electrohydrodynamic atomization (CEHDA)[17] can also yield layered bubble structures or even coat bubbles with macromolecules with control on the dispersitivity.[18] The underlying method is adaptable and robust because it can also be used to generate other interesting biomaterial morphologies such as particles, capsules, fibers, and tubes on the nano- and micrometer scales.[19−21] The fundamental aspects of such processing are driven by the application of an electric field on flowing media.[22] There are several additional benefits of such processing, including ambient temperature forming relatively coarse capillaries (reduced media blockage), high output rate, ease of assembly, and parametric control during forming (size and shape) and the option to scale up has already been demonstrated.[17,23]

■ MATERIALS AND METHODS

Materials. Bovine serum albumin (BSA) is a model protein[24] that has been utilized in numerous studies in the fabrication of device coatings,[25] scaffolds,[26] and bubbles,[27] which can also serve as an indicator for the utilization of other protein-based biomacromolecules. BSA (>96.0% lyophilized powder, essentially fatty-acid-free, and globulin-free), phosphate-buffered saline (PBS) (1 tablet in 200 mL of distilled water forms 137 mM NaCl, 2.7 mM KCl, and 10 mM phosphate buffer solution), ethanol (97.7%), terephthaloyl chloride (TCL) (≥99%), *m*-xylene (≥99.0%), catechol (≥99%), hydrogen peroxide (97%), and isopropanol-HCl (absolute isopropanol containing 0.04 M HCl) were all purchased from Sigma-Aldrich (Dorset, U.K.). L929 mouse fibroblast cells were obtained from The Foot and Mouth Disease Institute (Ankara, Turkey), and [3-(4,5-dimethylthiazol-2-yl)-2,5-diphenyltetrazolium bromide] (MTT) was purchased from Aldrich (St. Louis, Missouri, USA). Growth medium consisting of Dulbecco-modified medium supplemented with fetal calf serum, penicillin, streptomycin, and trypsin-EDTA was purchased from Biochrom (Berlin, Germany).

Methods. *Solution Preparation.* From previous studies, BSA has been utilized alongside PBS in the preparation of protein solutions.[28] However, it has been shown that using a secondary solvent such as ethanol can reduce the surface tension, which makes solutions more adaptable for electrohydrodynamic processing.[29] Furthermore, ethanol has been used in several biomaterial forming processes due to significantly reduced potential toxic effects when compared with other solvents. Other studies using BSA as a biosensor membrane,[28] utilized a 20 wt % BSA concentration, which was the lowest value we selected. Hence 20, 25, and 30 wt % BSA solutions were prepared using PBS, followed by the addition of 5, 10, and 15 v/v % ethanol to each BSA solution to determine the optimal processing concentration. Solutions were mechanically stirred for 2 h at the ambient temperature (23 °C). TCL (1 wt %) cross-linking agent was dissolved in xylene and stirred for 2 h at the ambient temperature in a sealed container. TCL has been previously used as a cross-linker to form BSA protein membranes and would allow a direct comparison with a simplistic forming method[28] without the use of bubbles. The analyte stock solutions of catechol and hydrogen peroxide were prepared using PBS with concentrations of 0.1 M.

Solution Characterization. BSA solutions and base solvents were characterized for their density, surface tension, viscosity, electrical conductivity, and pH immediately after preparation. The densities of the samples were estimated using a standard 10 ml density bottle (VWR International, Bedfordshire, U.K.). The static surface tension was measured using a Kruss tensiometer K9 (Krüs GmbH, Hamburg, Germany). For this, the plate method was used and the surface tension was recorded at the ambient temperature. Solution surface tension was measured just prior to processing. Electrical conductivity was assessed using a HACH SensION 156 dip-probe (Camlab, Cambridge, U.K.). The pH was measured using a pH meter (HANNA pH 21 pH/mV meter). The viscosity was calculated using the u-tube (VWR International, Bedfordshire, U.K.) method. All measurements were performed at ambient temperature (23 °C).

Experimental Setup. The CEHDA setup utilized[18] in the preparation of bubbles is illustrated in Figure 1a. Air was infused

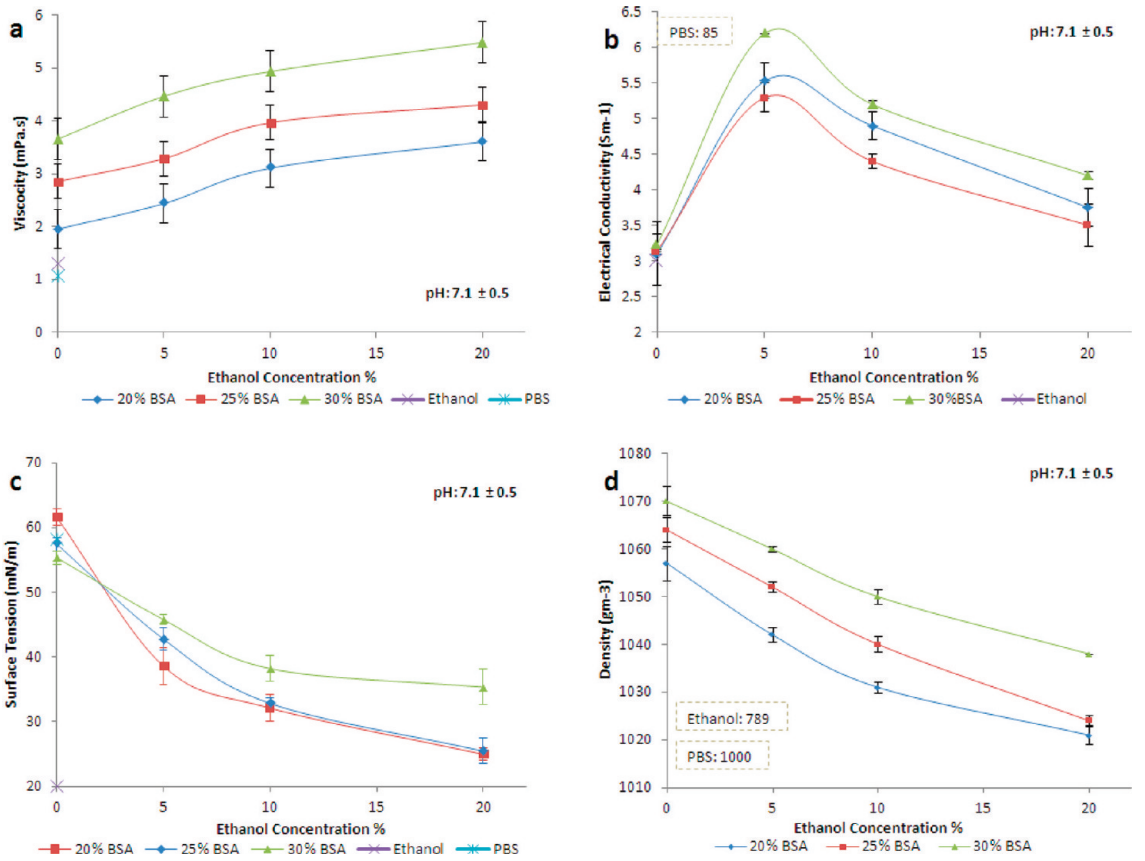

Figure 2. (a) Viscosity, (b) electrical conductivity, (c) surface tension, and (d) density of BSA solutions and solvents used in this study with their respective error bars.

through the inner nozzle (1.9 mm) of the stainless-steel coaxial device and BSA solutions were infused through the outer nozzle (2.2 mm) using Harvard precision syringe pumps (Edenbridge, U.K.). Both media were allowed to flow simultaneously. At a given combination of infusion rates, air becomes encapsulated in the BSA solution at the orifice, forming macroscopic scaled bubbles. Bubbling was enhanced by subjecting the flow to an electric field using a voltage source attached to the coaxially aligned needles (Glassman, Bramley, U.K.) producing a focusing effect on the gas/liquid, and hence a reduction in the size of bubbles obtained. The optimal values for the flow rate and applied voltage for stable bubble production were determined, and the diameters of the resulting bubbles were recorded, as described below.

Sample Collection. For preliminary analysis and determination of the optimal settings, bubbles were collected on glass slides with and without the use of the cross-linker and examined using an optical microscope to determine their size distribution. For membrane formation, bubbles were collected on a Petri dish onto a precoated thin layer of xylene and cross-linker. As the BSA bubbles were deposited on to the Petri dish homogenously, interfacial linking resulted between the reactive groups.

Non-microbubbled membranes were formed by layering the required organic and aqueous solution phases in a 5 ml beaker to create a stable interface. The BSA solution with different concentrations of ethanol was first introduced into the beaker; subsequently, xylene with cross-linking agent was carefully layered over the aqueous phase, as xylene has a lower specific gravity (0.88 at 20 °C). An immediate, solid, self-limiting membrane phase was formed at the liquid interface. The membrane surface area was sufficiently large to be readily handled and was detached from the wall of the beaker; generally membranes were removed after 12 h aging in the beaker. For subsequent use, the membranes were washed thoroughly in PBS, followed by distilled water to remove buffer residues.

For scaffold formation the bubbles were collected in a beaker with the xylene and cross-linker, exposing the structures completely to the active reagents. The bubbles were sprayed continuously until a 3D structure had evolved. All bubbles were collected at a distance of 80 mm from the orifice of the needle at ambient temperature (23 °C). The mechanism of cross-linking is shown in Figure 1b.

Bubble Characterization. Bubbles and their resulting structures were observed using a Nikon Eclipse ME600 optical microscope. In addition, Fourier-transform infrared spectroscopy (Nicolet-800FTIR) and scanning electron microscopy (Hitachi S-3400N SEM) were utilized to assist in structural characterization. For amperometric measurements, a μ-Autolab potentiostat (Eco Chemie, Utrecht, The Netherlands) was used.

Membrane Diffusivity Measurements. Experimental details of membrane diffusion measurements are found elsewhere.[28] Membranes formed using bubble templates were assessed for their diffusion properties using a planar platinum working electrode (Rank Brothers, Cambridge, U.K.). To measure analyte diffusion through the membranes, we cut 16 mm × 16 mm sections from various areas of the membrane to ensure reliability and accuracy and placed them over the planar electrode covering the sensing surface. The electrochemically active analytes diffused through were hydrogen peroxide and catechol, measured at a polarizing voltage of +0.65 V over the working electrode versus the Ag/AgCl reference electrode. The electrode response was then measured by the current change due to surface redox reaction for each of the analytes studied. All membranes analyzed were less than one tenth of thickness of the working electrode diameter (<200 μm) and therefore considered to be suitable to avoid any edge effects.

Cellular Activity on Protein Scaffolds (MTT Assay). L929 Mouse fibroblast cell lines were used for cell testing. The scaffolds and the control vial substrate were cut identically and immersed in the cell culture medium and incubated (Revco Technologies, Asheville, NC) under humidified 5% CO_2/95% air environment at 37 °C. We pipetted 50 μl of medium with the concentration of 8000 cells/ml into each sample well.

dx.doi.org/10.1021/bm201202y|*Biomacromolecules* 2011, 12, 4291–4300

At the end of 1, 4, and 7 days, the medium was replaced with 100 μl of fresh medium and 13 μl of MTT solution. After 4 h of incubation in the dark at 37 °C, the medium was removed again and 200 μl of isopropanol-HCl was added to each well to dissolve the formazan crystals. After 10 min, the wells were read on a 570 nm ELISA plate reader (Asys-UVM-340), and the percentage of cell viability was calculated. Cell viability was defined as 100% for the MTT assay control, and cell growth was directly proportional to the absorbance at a wavelength of 570 nm. The morphological characteristics of the cells cultured onto the scaffolds were also investigated. L929 mouse fibroblast cells were seeded on the scaffolds and incubated at 37 °C for 1 day. Following the incubation, scaffolds were washed with PBS three times. Loosely adherent or unbound cells were removed and scaffolds were fixed with May Grunwald-Giemsa for 300 s and washed with PBS, and the samples were then stained with methylene blue that was diluted in the ratio of 1:2 with PBS for 10 min for optical microscopy analysis.

RESULTS AND DISCUSSION

Solution Properties. The physical properties of the processing solutions have a significant effect upon the jetting behavior observed during electrohydrodynamic fabrication of structures. Specifically, they can lead to a mode preference in the microbubbling process, which can be displayed in the overall parametric map[17,20] of flow rate against applied voltage. Three different BSA concentrations (20, 25, and 30 wt %) were assessed at the ambient temperature (23 °C), and the role of overall ethanol concentration on the physical properties of these solutions was determined. From previous studies, it is known that solutions prepared from ethanol are well-suited[29] for electrohydrodynamic processing of this form due to its relatively low surface tension when compared with water. Figure 2 shows the solution properties of the solvents and solutions used. The viscosity (Figure 2a) of all solutions (20, 25, and 30 wt % BSA) increased slightly as the ethanol concentration increased. As expected, at fixed ethanol concentrations, an increase in the BSA content resulted in an increase in the viscosity. For example, at an ethanol concentration of 5%, when 20 wt % BSA was incorporated, the mean viscosity was ~2.3 mPa s. When the BSA content was increased from 20 to 30%, the viscosity increased to ~4.3 mPa s. Similar trends were observed for all ethanol concentrations. This can be attributed to the increase in molecular interactions at higher concentrations.[30] The increase in viscosity due to an increase in BSA concentration was more marked than those observed for changes to ethanol concentration.

Figure 2b shows the effect of ethanol concentration (in BSA solutions) on the electrical conductivity. All solutions containing ethanol demonstrated greater electrical conductivities that those that did not have ethanol. However, the electrical conductivity of solutions containing ethanol was the greatest at the lowest ethanol concentration (5%), which then reduced on further increments of ethanol (10 and 20%).

The addition of ethanol to the various BSA solutions reduces the overall surface tension of the solution; this is desirable because high surface tension retards the possibilities of electrohydrodynamic processing, although methods have been developed to overcome this problem (Figure 2c).[31] All surface tension values for ethanol containing BSA solutions were below 50 mN m^{-1}, which makes them suitable for the proposed processing routes. The density of all BSA solutions decreased as the ethanol content increased (Figure 2d), as expected, which is due to ethanol possessing a lower density than PBS solution, which was used to make up the remaining volumes for individual BSA solutions.

Effect of Ethanol on Proteins. The effect of ethanol on various protein solutions can be observed by studies carried out on the effect on foaming properties.[32,33] It has been demonstrated that the addition of small amounts of ethanol increase foam stability due to the sharp reduction in surface tension of the aqueous protein solution, and this phenomenon is associated with the formation of smaller gas bubbles and reduced bubble coalescence. However, because of protein's susceptibility to change in several processing routes, determining the optimal ethanol concentration is of great importance because higher ethanol concentrations may lead to foam instability along with the aggregation of proteins in bulk solutions associated with denaturation.[34] To demonstrate the feasibility, the lowest BSA solution (20 wt %) was selected as the stock solution, and known quantities of ethanol were added to prepare 0, 5, 10, and 20% solutions in relation to PBS. Membranes were prepared by simple casting. FTIR studies performed on membranes (Figure 3a) revealed absorption bands as expected from a native BSA at the regions of amides 1 (~1650 cm^{-1}) and 2 (~1500 cm^{-1}).

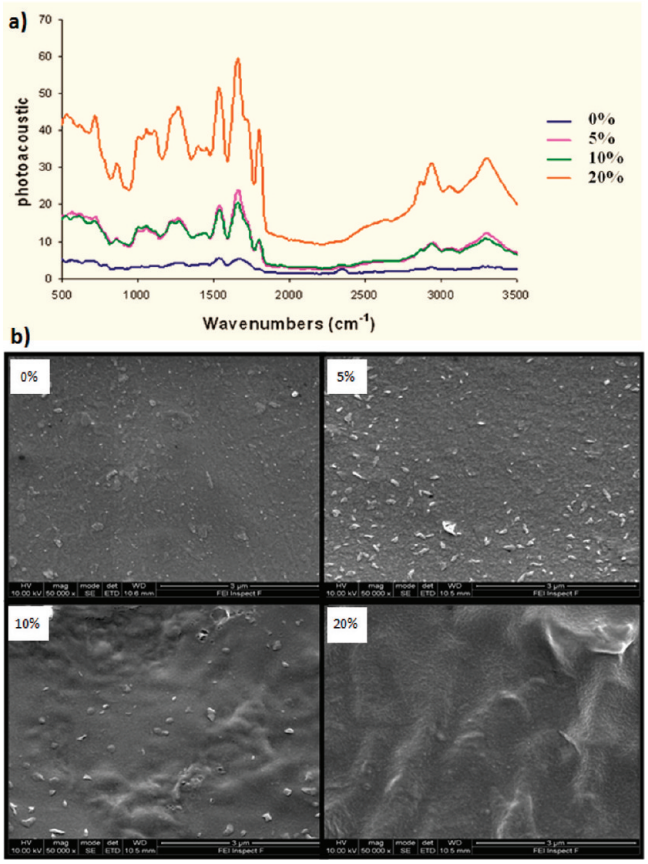

Figure 3. (a) FTIR photoacoustic (in arbitrary units) spectra of 20 wt % BSA membranes prepared using different concentrations of ethanol (0, 5, 10, and 20%) and corresponding (b) electron micrographs of membrane structures.

SEM results (Figure 3b) from various films indicated no significant effect of ethanol concentration apart from the rougher surface seen with higher concentrations due to the increased drying effect from the ethanol. The more rapid evaporation leads to non-uniform aggregation of the polymer.

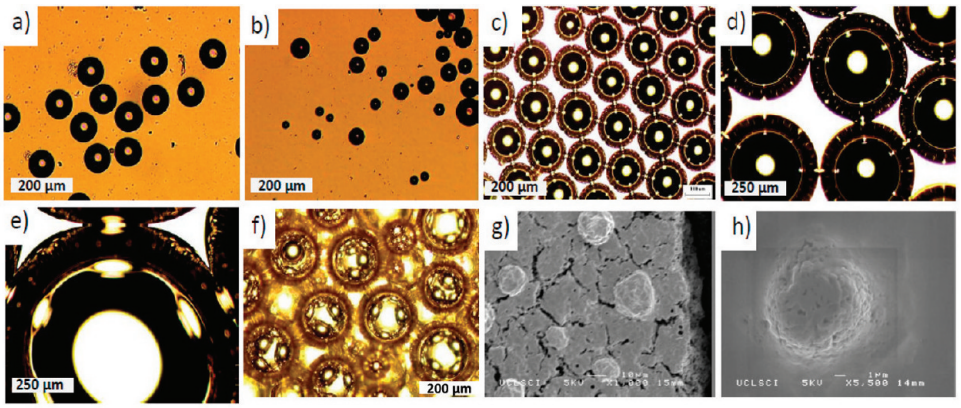

Figure 4. BSA microbubbles prepared using electrohydrodynamic flow and a 20 wt % BSA solution (including 10% ethanol v/v) showing: (a) BSA bubbles (100 μm), (b) bubble size after diffusion, and (c) single-layered BSA bubbles (~100 μm in diameter). BSA bubbles with approximate diameters of (d) 300 and (e) 900 μm. (f) Multilayered bubble structure. Structures after diffusion from (g) pure BSA and (h) partially cross-linked BSA bubbles.

The films were cast on glass coverslips (22 × 22 × 0.1 mm) for SEM. The surface structure under SEM was uniform throughout with small residual white salt particles (from the PBS solution).

Microbubbling Process and Collection Method. We selected 20 wt % BSA (10% v/v ethanol) to demonstrate microbubble fabrication. This BSA concentration has been used with other techniques for thin film production.[28] Additional concentrations of 25 and 30 wt % BSA were utilized to generate and compare 3D scaffolds. The jetting modes[35,36] are vital features in electrohydrodynamic atomization during spraying and spinning processes; however, in the microbubbling process, these take on distinctly different features due to high air flow interaction and encapsulation.[17] The necessity of high air infusion rates hinders cone-jet formation. To enable microbubble production, we commonly encounter three different modes of bubbling.. The initial bubble dripping mode, where air and the protein solution are allowed to flow simultaneously without the application of voltage, results in bulky droplets of air encapsulated with BSA. At this point, the bubbles generated are very coarse; in fact, they are comparable to the processing needle diameter and are highly polydisperse. This stage is of significance because it establishes concentric air−media coflow, leading to further modes on the application of the driving voltage. Once the voltage is applied, coflowing air and BSA enter the coning mode in the microbubbling process. Further increasing the voltage leads to the microbubbling mode whereby a near stable mode is established, resulting in even finer bubbles. The sizes of bubbles can be adjusted by varying the infusion rates of BSA solution and air, the applied voltage, and the collection distance.[18] As well as being able to optimize the processing parameters, the solution parameters can also be optimized to achieve desired bubble size and distribution. Here, using the selected BSA solution, the microbubbling mode was achieved and the operating window was primarily determined by means of experimentation by varying the processing parameters. Because of the cross-linking process, the collection method also plays an extremely crucial role when fabricating desired structures.

Changes to protein microbubble processing with respect to parameters were determined and kept within the optimized parametric range for both the applied voltage (7−14 kV) and media flow rates (outer needle BSA: 400−500 μl/min, inner needle air: 3000−4000 μl/min). The initial collecting distance was fixed at 200 mm. Figure 4a shows microbubbles (~100 μm) prepared using the 20 wt % BSA solution (flow rate BSA: 400, air: 3000 μl/min) and an inclusive applied voltage range of 12−13 kV. During this process, as is the case with other electrically driven processes (e.g., electrospinning and electrospraying), instabilities were encountered, which are due to electrostatic changes in the environment. Over a time period of 10 min the size of these bubbles reduced because of gaseous diffusion (Figure 4b), which also suggests that the rate of gas diffusion from each bubble may vary. To achieve a monolayered structure, we can collect bubbles in a controlled fashion by reducing the deposition distance to the substrate, from 200 to 100 mm, (Figure 4c), which subsequently gives rise to the desired structures (~150 μm). For a given optimized parametric set (in this case with microbubbles ~150 μm), the polydispersivity index is calculated to be ~6%, which is considerably lower than values obtained for sonication (~150%).[18] This enables a compact collecting zone, allowing concentrated bubble deposition. The size of these structures can be reduced by straightforward controllable means and by reducing the applied voltage, which is a crucial variable in such processes; the size of bubbles can be increased significantly. For example, reducing the applied voltage to 10−11 kV causes an increase in protein bubble size (~300 μm, Figure 4d) but can also be increased further if the applied voltage range is reduced to 7−9 kV (~950 μm, Figure 4e). Whereas the applied voltage can deliver systematic reduction in bubble morphology, the process is governed by an electric field, surface tension, and gravitational forces, which give rise to jetting stability and modes. Hence, for such processes, mode-mapping can visually define numerical points where such parameters become null due to transitions toward unwanted modes, for example, dripping.[36]

By maintaining the reduced collection distance, thus confining the collecting plane, to 100 mm, monolayered structures eventually become multilayered structures (Figure 4f), while maintaining bubble integrity. In spraying and spinning processes the collecting or deposition distance plays a role in the resulting morphology size,[35] however, this does not seem to be as influential during the bubbling process in this work, as structures collected at both distances (100 and 200 mm) were similar in size but differed in density. Bubbles left

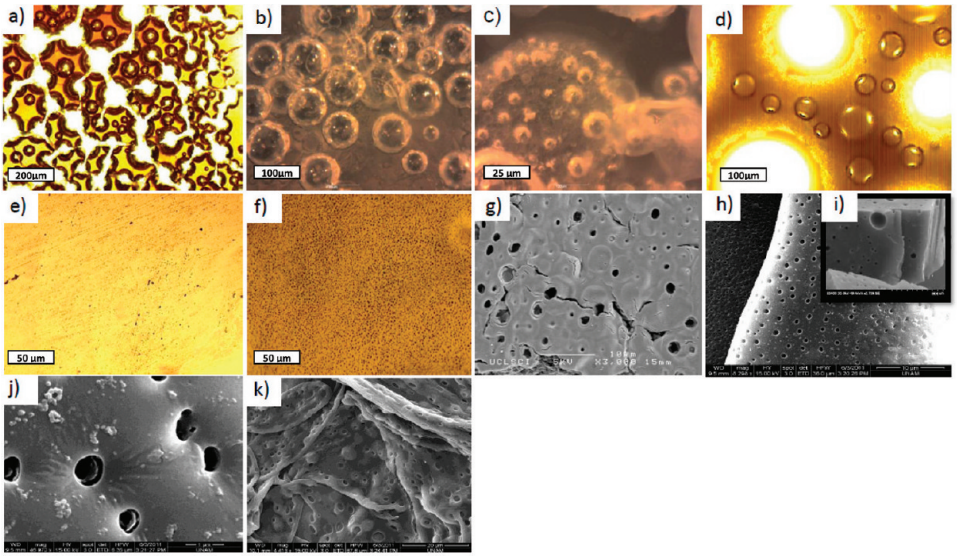

Figure 5. Preparation of BSA membranes (using 20 wt % BSA): (a) non-cross-linked BSA film, (b) randomly orientated cross-linked bubbles, (c) smaller bubbles at parent bubble-BSA surface, and (d) lodged bubble template. Membrane structures using (e) electrosprayed BSA, (f) BSA bubbles, (g) magnification of bubbled membrane, (h) cross-linked and bubbled membranes with inset (i) showing edge of membrane, (j) magnification of pores formed using cross-linker and microbubbling, and (k) membrane morphology when using 30 wt % BSA and 20% ethanol (v/v).

undisturbed were seen to collapse after undergoing shrinkage (diffusion) at various time points. However, some bubbles did not collapse and continued to shrink, resulting in speck-like features under an optical microscope. Observing these structures under electron microscopy reveals particles resulting from gas diffusion from bubbles, which are found on top of dried protein, which arises from collapsed and surface dissolved bubbles (Figure 4g). These are between 8 and 20 μm in size, but because they are a function of bubble coating, using a lower loading volume of BSA on the bubble surface[18] can effectively give rise to smaller particles formed via gas diffusion. By partially cross-linking bubbles (collecting them on a very thin layer of TCL in xylene), the surface of these structures can be altered to alter the porosity (Figure 4h). In previous studies, microbubbles have been used as pore-generating devices[13] but without the assistance of a cross-linker. In this instance, as the BSA is partially cross-linked at the bubbles base, the diffusion of gas from the bubbles inner core is restricted and results in increased polymer interaction at the base, leading to an increase in pressure. This could give rise to pores, which are formed due to diffusion. Another possibility pertains to the cross-linking effect. The bubbles base is cross-linked, which yields greater adhesion between BSA molecules at this location, causing changes in pressure. Such changes may lead to spontaneous bubble formation, giving rise to such pores.[37] Finally, the evolution of HCl, as a by-product of the cross-linking reaction, may also contribute toward pore generation.

In relation to achieving smaller scaled architectures using such processes, several routes exist, and these include using finer needles.[38] Although the achievable scale is acceptable, bubble structures generated on this scale are currently non-uniform.[17] Alternatively, smaller daughter structures can be achieved by natural means using secondary bubble structures that are formed as a result of controlled bubble break down.[39]

Membrane Formation. One technique that uses interfacial polymerization of albumin in the production of membranes is microfluidics. However, the downside is that the membrane produced is not permeable to some common molecules such as ammonia.[28] The objective behind attaining a porous membrane is to enable microsolute transport, for example, to cells. This is achievable by introducing a bubble system into the membrane during in-situ formation.

Using monolayered bubbles (prepared using the same BSA solution, with controlled variations in the ethanol content, 5 and 10% v/v and parameters deployed for microbubble formation), the fabrication of porous protein films is possible. However, the process requires a cross-linker as films formed from densely populated monolayered bubbles fracture due to the drying process (Figure 5a). By using TCL as the collecting substrate, bubbles can be readily cross-linked and solidified once totally submerged in the solution (Figure 5b), thus signifying their potential as a template. On closer inspection of bubbles collected toward the surface of the cross-linking solution, with very short contact in the cross-linker (Figure 5c), the presence of smaller bubbles is apparent on the surface. These structures appear during the cross-linking process because they would not have formed after BSA solidification and again can be attributed to the spontaneous nucleation of smaller bubbles or evolution of HCl gas from the cross-linking reaction. Furthermore, Figure 5d shows a monolayered film that again has minimal contact with the cross-linking solution. In this instance, a template remains from the initial bubble structure, but between the windows struts, remnants of smaller bubble templates can be observed.

To determine the role of bubbles in the formation of pores in BSA structures, we switched the microbubbling process to electrohydrodynamic spraying mode using the same processing device. The infusion of air in the processing outlet was switched off, and BSA was electrosprayed (flow rate: 40 μl/min, applied voltage: 9.3 kV) on to a glass slide. Optical analysis (Figure 5e) confirms the absence of pores. However, when a membrane is allowed to form using a monolayered bubble template, pores are present, which favors the role of bubbles over HCl accumulation (by-product during cross-linking) in achieving this feat (Figure 5f). Electron micrographs of the BSA bubble template membranes confirm the presence of pores, ranging

from 1 to 5 μm (Figure 5g), but the structure is also fractured intermittently. Cross-linking is used to improve the surface consistency and in this process is performed by using a very thin layer of cross-linker at the base of the collecting substrate. When formed using the microbubbling process, in conjunction with cross-linking, membranes are porous (Figure 5h). The pores display a near-monodisperse size distribution, and these pores extend throughout the membrane structure (Figure 5i), and on closer inspection, the size of these pores has an average pore diameter of 300 nm (standard deviation: 60 nm) (Figure 5j). The base of the membrane is solid and non-porous, which is where the bulk of the cross-linker is located and where the reaction is initiated from. It is worth noting that when the highest BSA concentration (30 wt %) is used in conjunction with the high quantities of ethanol (20% v/v) the pore structure is compromised, as is the surface uniformity of the membrane (Figure 5k). Also, differences in pore sizes arise in uniform films from changes in ethanol concentration in initial BSA processing solutions. Ten v/v % ethanol BSA solutions have an average pore size of 1.35 μm (standard deviation: 340 nm).

The membrane was readily detachable, and the thicknesses were measured using light microscopy by mounting them between glass coverslips and measuring the refractive index at glass surfaces. Diffusion properties of both membranes were analyzed and compared with previous studies utilizing the same materials but a different processing route.

Diffusion Properties of Formed Membranes. To identify the behavior and transport properties of these protein membranes, diffusion properties were studied. A membrane covering electrode technique was performed with an assumption of solute diffusion following Fick's law. Membranes were exposed; a step change in diffusant concentration and the resulting amperometric currents were recorded. The diffusion coefficients of model solutes, catechol, and hydrogen peroxide through the membranes were measured by fitting simulated amperometric currents to experimental data. A typical fit of catechol diffusion through a cross-linked BSA (with 10% v/v ethanol) bubble membrane is shown in Figure 6a. Because the diffusion coefficient was determined through a multiple data set of the time-dependent on electrode response, the accuracy was enhanced. The standard deviation for the normalized amperometric currents in Figure 6a is <0.01. The method thus gives an exceptionally precise and readily validated measure of the diffusion coefficient. Any differences in measured diffusion coefficients are, therefore, an indication of true differences between membranes.

Typical amperometric current response profiles for catechol and hydrogen peroxide are shown in Figure 6b,c. It can be seen that the amperometric current for hydrogen peroxide reaches a plateau response earlier than that of catechol. The hydrogen peroxide thus has a higher diffusivity than catechol. This is further seen by calculating the diffusion coefficients from the response profiles. There appears to be a relationship between transfer of these neutral species and their molecular weights (hydrogen peroxide, 16; catechol, 110). These values are consistent with the diffusion coefficients obtained using microfluidics.[28] The higher overall diffusivity observed with 10% v/v ethanol cross-linked BSA bubble membrane supports a penetrating pore structure.

The generated thicknesses of 5 and 10 v/v % ethanol BSA bubble membranes were 81 and 78 μm, respectively. The 5 v/v % ethanol BSA bubble membrane displays a less permeable

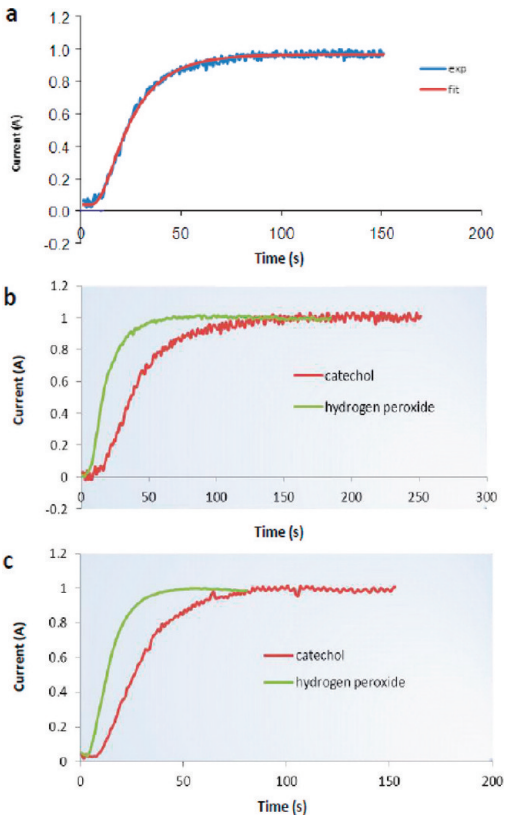

Figure 6. Diffusion across membranes. (a) Normalized experimental (solid diamond blue) and simulated (solid square red) transient amperometric currents for catechol diffusion through cross-linked BSA (5 wt % ethanol) bubble membrane. Amperometric responses with (b) 5% ethanol and (c) 10% ethanol.

structure due to either a denser, tightly cross-linked network or the rapid gas diffusion from bubbles forming the pores. The diffusivities of hydrogen peroxide and catechol through the 10% v/v ethanol BSA bubble membranes were (6.2 and 2.6) $\times$ 10^{-7} cm^2 s^{-1}, respectively, which are higher than those for the 5% ethanol BSA bubble membranes as (4.8 and 1.7) $\times$ 10^{-7} cm^2 s^{-1}, respectively. Undoubtedly, the 5% ethanol BSA bubble membrane was denser and less porous.

Scaffold Formation. Foam structures were used as scaffolds where microbubbles were collected in a 50 ml beaker, half-filled with the cross−linker. The difference between film and foaming methods is that the foaming method establishes a stable platform to prepare 3D scaffold structures using a bottom-up approach as the bubbles start to form a 3D network as chemical coupling occurs rapidly and throughout the microbubbled structures. In any case, unreacted BSA components were treated with the cross-linker manually once microbubbling was complete (<60 s).

This method utilized three different concentrations of BSA (20, 25, and 30 wt %) with a constant ethanol concentration of 10% v/v (Figure 7). As a control, for all three concentrations, BSA structures were generated within the same parametric window without the addition of ethanol and without cross-linking (Figure 7a1,b1,c1). A clear discrepancy is visible between the control and modified structures in terms of bubble and strut stability, homogeneity, and order. Porous structures generated using 20 wt % BSA displayed a mean pore diameter of 470 μm (Figure 7a2−a4). These interconnected macropores were dried under ambient conditions. The control

dx.doi.org/10.1021/bm201202y|Biomacromolecules 2011, 12, 4291−4300

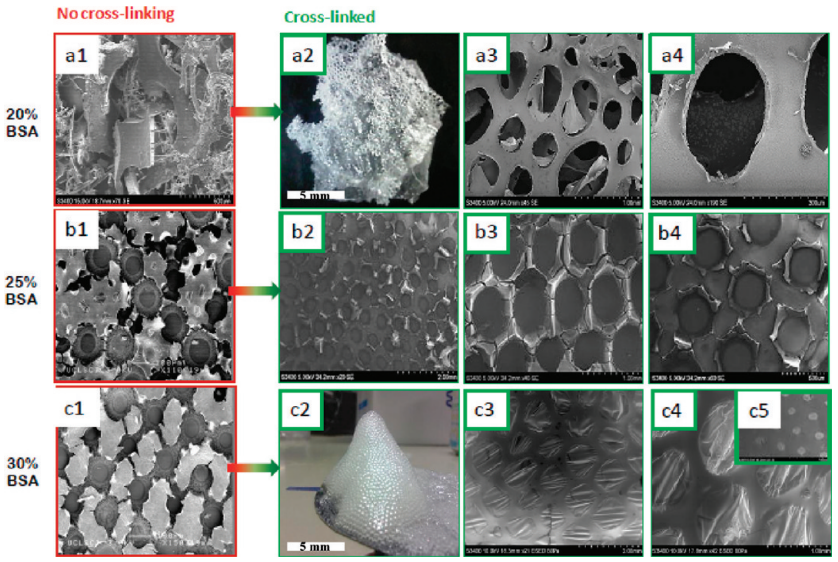

Figure 7. BSA scaffold preparation. (a1−a4) Structures prepared using 20% BSA. (a1) Non-cross-linked bubbles result in fractured structures and (a2−a4) showing scaffolds with open "windows". (b1,b2) Scaffolds prepared using 25% BSA. (b1) Non-cross-linked bubbles result in fractured structures and (b2−b4) showing scaffolds with open windows but extended tails on window edges. (c1−c4) Structures prepared from 30% BSA. (c1) Non-cross-linked bubbles and (c2−c5) scaffolds with closed windows.

for this concentration showed no difference in stability until drying, where BSA microbubbles collapsed or the strut/walls were too brittle upon drying, leading to fracture. When the concentration was increased to 25% there was not a significant change in mean pore size (430 μm) (Figure 7b2−b4); however, because of a more viscous solution, the shell thickness of the bubbles also increased, leading to a more coated strut formation and a rougher surface when compared with 20 wt % structures. Both open and closed pores were observed with the control along with non-uniform bubble production.

Finally, using 30 wt % BSA, a closed pore network was established with a mean pore size of 950 μm (Figure 7c2−c5). Again due to the increased viscosity (as a result of increased BSA concentration) increased cohesion results in thin film formation between struts, which are observed as closed windows rather than the desired open windows, which are crucial in tissue engineering structures.

Through varying the protein concentration of solutions and finding a balance between the protein, PBS, and ethanol concentrations, it is possible to vary the pore sizes along with the topography for enhancing cell attachment and other biological substances depending on the application. Closed window structures may be useful in delivering patterned topographies, which are known to enhance and control cellular attachment and proliferation.

Hence controlled parametric changes during bubble forming (voltage and selected media flow rate) can lead to changes in the size of bubbles, which will then result in corresponding pore sizes. Additionally, the layering will determine the overall size of the structure. By contrast, in other methods of preparing scaffolds the potential to control pore sizes also exists, but there are restrictions or drawbacks. For example, with conventional electrospinning[12] pore sizes are often compromised with the density of the structures, as fibers are randomly deposited over each other. With direct writing methods, the speed of forming is often a limiting factor[10] even though more porous complex structures can be achieved. Likewise, freeze-casting[9] can also afford complex porous structures, but is composed of numerous steps (e.g., casting, solidification, sublimation), which again has an impact on the output rate.

Cell Studies on 3D Protein Scaffolds. It is apparent that type of pore (open or closed systems) and pore size of bioscaffolds govern cell viability and proliferation. The results are in agreement with previous studies showing that larger pore size is directly linked to enhanced cell proliferation.[40] None the least, it is evident that closed pore systems further enhance cell proliferation due to possessing higher mechanical properties and the fact that cell adhesion is facilitated when compared with open pore systems due to a larger initial contact surface area. However, this is a compromising factor because open pore systems are very much suited for bioprocesses in regeneration as they are well-suited to providing integration throughout the scaffold device. However, as highlighted, the closed pore network can be used as a method of delivering controlled topographical pattering (on selected sides), which is rapidly emerging as an important cue in enhancing cellular attachment. Hence, although these structures are classed as scaffolds, this is certainly the case for the structures obtained with 20 and 25 wt % BSA, where the pores are open and ideal for integration (not shown in this study). With the 30 wt % structure, the regular closed-pore patterned surface can also be utilized (in addition to coatings for devices) as part of recently developed strategies in preparing and utilizing bilayered scaffolds.

Figure 8a shows the formazan absorption of L929 cells cultured for 1, 4, and 7 days. The data were evaluated against the formazan absorbance (mean ± standard deviation n = 8). All samples demonstrated an increase in cell proliferation with increased incubation time, and the results are statistically significant for all groups (p < 0,005). Up to the fourth day, 20 and 25 wt % BSA scaffolds showed no significant difference in the number of cell proliferation; this can be attributed to the scaffolds having similar pore sizes, but on the seventh day, increased concentration of BSA showed increased cell proliferation. Although the protein concentration of the scaffolds was increased in the same proportion, it is observed that initially the protein concentration does not have an

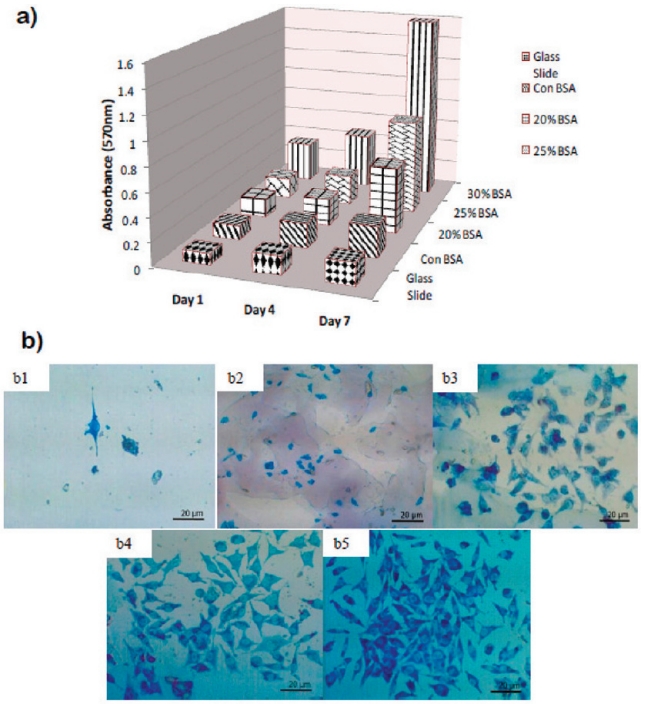

Figure 8. (a) Graph showing the proliferation of L929 mouse fibroblast cells cultured in media up to 7 days. Fibroblast proliferation was measured by methylene blue assay. (b) Opticals showing L929 cells cultured in media: (b1) glass slide only as control, (b2) untreated BSA scaffold, (b3) cross-linked 20 wt % BSA, (b4) cross-linked 25 wt % BSA,and (b5) cross-linked 30 wt % BSA for 24 h. The scale bar in each case is 20 μm.

instantaneous effect on cell proliferation but pore size and type (open or close) are driving factors, as the highest formazan absorbance was obtained from the cells cultured on 30 wt % BSA closed pore system structures for all days. Cell proliferation and spreading were observed using optical microscopy (Figure 8b). BSA scaffolds (30 wt %) showed a denser cell population compared to other concentrations, untreated BSA and glass slide.

CONCLUSIONS

Using a recently developed microbubbling process capable of preparing bubbles coated with biomacromolecules, in this case using model protein BSA, the potential to deliver a broad range of generic biomaterials is demonstrated. The process is versatile and robust, and in conjunction with chemical modification of BSA (using a cross-linker), bubble structures, films, porous films, scaffolds, and enhanced surfaces can be generated. The application of such structures is demonstrated for bubbles, biosensor, and tissue engineering applications. The method is a one-step process (including deposition directly into desired media), which can benefit several remits of the aforementioned fields. In addition, the process is robust and makes use of bubbles as novel tools in advancing these fields. Finally, BSA protein can be readily substituted with other biomacromolecules to yield similar structures that can be highly beneficial for several applications.

AUTHOR INFORMATION

Corresponding Author

*E-mail: zeeshan.ahmad@port.ac.uk.

ACKNOWLEDGMENTS

We would like to thank UCL Archaeology Department for the use of their electron microscopes. We would also like to thank UCL for partially funding Z.E.'s Ph.D.

REFERENCES

(1) Sosnowski, S.; Wozniak, P.; Lewandowska-Szumiel, M. *Macromol. Biosci.* **2006**, *6*, 425−434.
(2) Billon, L.; Manguian, M.; Pellerin, V.; Joubert, M.; Eterradossi, O.; Garay, H. *Macromolecules* **2009**, *42*, 345−356.
(3) Nystrom, D.; Antoni, P.; Malmstrom, E.; Johansson, M.; Whittaker, M.; Hult, A. *Macromol. Rapid Commun.* **2005**, *26*, 524−528.
(4) Izquierdo, R.; Garcia-Giralt, N.; Rodriguez, M. T.; Caceres, E.; Garcia, S. J.; Gomez Ribelles, J. L.; Monleon, M.; Monllau, J. C.; Suay, J. *J. Biomed. Mater. Res., Part A* **2008**, *85A*, 25−35.
(5) Ko, Y.-G.; Kawazoe, N.; Tateishi, T.; Chen, G. *J. Bioact. Compat. Polym.* **2010**, *25*, 360−373.
(6) Wood, C. D.; Tan, B.; Lee, J.-Y.; Cooper, A. I. In *Gas-Expanded Liquids and near-Critical Media: Green Chemistry and Engineering*; Hutchenson, K. W., Scurto, A. M., Subramaniam, B., Eds.; American Chemical Society: Washington, DC, 2009; Vol. *1006*, pp 243−258.
(7) Carletti, E.; Endogan, T.; Hasirci, N.; Hasirci, V.; Maniglio, D.; Motta, A.; Migliaresi, C. *J. Tissue Eng. Regener. Med.* **2011**, *5*, 569−577.
(8) Barbetta, A.; Massimi, M.; Di Rosario, B.; Nardecchia, S.; De Colli, M.; Devirgiliis, L. C.; Dentini, M. *Biomacromolecules* **2008**, *9*, 2844−2856.
(9) Mallick, K. K. *J. Am. Ceram. Soc.* **2009**, *92*, S85−S94.
(10) Ahmad, Z.; Huang, J.; Thian, E. S.; Edirisinghe, M. J.; Jayasinghe, S. N.; Best, S. M.; Bonfield, W.; Brooks, R. A.; Rushton, N. *J. Biomed. Nanotechnol.* **2008**, *4*, 185−195.
(11) Liu, J.; Morykwas, M. J.; Argenta, L. C.; Wagner, W. D. *J. Biomed. Mater. Res., Part B* **2011**, *98B*, 316−322.
(12) Pham, Q. P.; Sharma, U.; Mikos, A. G. *Biomacromolecules* **2006**, *7*, 2796−2805.
(13) Nair, A.; Thevenot, P.; Dey, J.; Shen, J. H.; Sun, M. W.; Yang, J.; Tang, L. P. *Tissue Eng., Part C* **2010**, *16*, 23−32.
(14) Wang, W. H.; Moser, C. C.; Wheatley, M. A. *J. Phys. Chem.* **1996**, *100*, 13815−13821.
(15) Unger, E. C.; Porter, T.; Culp, W.; Labell, R.; Matsunaga, T.; Zutshi, R. *Adv. Drug Delivery Rev.* **2004**, *56*, 1291−1314.
(16) Stride, E.; Edirisinghe, M. *Soft Matter* **2008**, *4*, 2350−2359.
(17) Farook, U.; Stride, E.; Edirisinghe, M. *J. R. Soc. Interface* **2009**, *6*, 271−277.
(18) Ekemen, Z.; Ahmad, Z.; Edirisinghe, M.; Stride, E. *Macromol. Mater. Eng.* **2011**, *296*, 8−13.
(19) Wu, Y.; MacKay, J. A.; McDaniel, J. R.; Chilkoti, A.; Clark, R. L. *Biomacromolecules* **2009**, *10*, 19−24.
(20) Enayati, M.; Ahmad, Z.; Stride, E.; Edirisinghe, M. *J. R. Soc. Interface* **2010**, *7*, 667−675.
(21) Chakraborty, S.; Liao, I. C.; Adler, A.; Leong, K. W. *Adv. Drug Delivery Rev.* **2009**, *61*, 1043−1054.
(22) Hayati, I.; Bailey, A. I.; Tadros, T. F. *Nature* **1986**, *319*, 41−43.
(23) Bocanegra, R.; Galan, D.; Marquez, M.; Loscertales, I. G.; Barrero, A. *J. Aerosol Sci.* **2005**, *36*, 1387−1399.
(24) *Albumin Structure, Function and Uses*; Rosenoer, V. M., Oratz, M., Rothschild, M. A., Eds.; Pergamon Press: Oxford, U.K., 1977; pp 255−273.
(25) Wen, H. B.; de Wijn, J. R.; van Blitterswijk, C. A.; de Groot, K. *J. Biomed. Mater. Res.* **1999**, *46*, 245−252.
(26) Jaklenec, A.; Wan, E.; Murray, M. E.; Mathiowitz, E. *Biomaterials* **2008**, *29*, 185−192.
(27) Grinstaff, M. W.; Suslick, K. S. *Proc. Natl. Acad. Sci. U. S. A.* **1991**, *88*, 7708−7710.
(28) Chang, H.; Khan, R.; Rong, Z.; Sapelkin, A.; Vadgama, P. *Biofabrication* **2010**, *2*, 035002.
(29) Pareta, R.; Brindley, A.; Edirisinghe, M. J.; Jayasinghe, S. N.; Luklinska, Z. B. *J. Mater. Sci.: Mater. Med.* **2005**, *16*, 919−925.

(30) Yadav, S.; Shire, S. J.; Kalonia, D. S. *Pharm. Res.* **2011**, *28*, 1973−83.
(31) Stachewicz, U.; Yurteri, C. U.; Dijksman, J. F.; Marijnissen, J. C. M. *J. Aerosol Sci.* **2010**, *41*, 963−973.
(32) Ahmed, M.; Dickinson, E. *Colloids Surf.* **1990**, *47*, 353−365.
(33) ElyseeCollen, B.; Lencki, R. W. *Biotechnol. Prog.* **1997**, *13*, 849−856.
(34) Militello, V.; Casarino, C.; Emanuele, A.; Giostra, A.; Pullara, F.; Leone, M. *Biophys. Chem.* **2004**, *107*, 175−187.
(35) Enayati, M.; Chang, M. W.; Bragman, F.; Edirisinghe, M.; Stride, E. *Colloids Surf., A* **2011**, *382*, 154−164.
(36) Jaworek, A.; Krupa, A. *J. Aerosol Sci.* **1999**, *30*, 873−893.
(37) Fukasawa, Y.; Chen, J.; Saito, H. *J. Polym. Sci., Part B: Polym. Phys.* **2008**, *46*, 843−846.
(38) Park, J.-U.; Hardy, M.; Kang, S. J.; Barton, K.; Adair, K.; Mukhopadhyay, D. K.; Lee, C. Y.; Strano, M. S.; Alleyne, A. G.; Georgiadis, J. G.; Ferreira, P. M.; Rogers, J. A. *Nat. Mater.* **2007**, *6*, 782−789.
(39) Bird, J. C.; de Ruiter, R.; Courbin, L.; Stone, H. A. *Nature* **2010**, *465*, 759−762.
(40) Kim, H. J.; Kim, U. J.; Vunjak-Novakovic, G.; Min, B. H.; Kaplan, D. L. *Biomaterials* **2005**, *26*, 4442−4452.